

Supplement of “The grain-scale signature of isotopic diffusion in ice” by Felix S. L. Ng

Contents

Movies S1–S7 [Captions only in this file. Please access the movies via doi:10.15131/shef.data.25513414]

5 Section S1: Matrix M in our numerical method (including Fig. S1)

Section S2: Effect of reducing the signal wavelength to 2 cm (including Figs. S2 and S3)

Section S3: Effect of vein-water flow on the archetypal patterns (including Figs. S4 and S5)

Section S4: Effect of grain radius b larger than 1 mm (including Figs. S6–S10)

Figure S11

10

15

20

25

30

Movie captions

Movie S1. Evolution of horizontal isotopic pattern with depth in the simulation with $T = -32\text{ }^{\circ}\text{C}$, $\lambda = 10\text{ cm}$, $c = 5\text{ nm}$, $w = 0\text{ m yr}^{-1}$, and $D_b = 1.5 \times 10^{-12}\text{ m}^2\text{ s}^{-1}$ (medium-high diffusivity run in Fig. 4b), compiled by sampling the normalised δ -variations in the ice annular domain at different z . (a) Depth profiles of the δ -variations at the mid-grain interior (black), grain-boundary interior (blue), and vein wall (red) over a signal wavelength. The black curve is overlain by the blue curve in this run. Dashed line marks the depth being sampled. (b) Isotopic patterns, shown with the same colour scheme as in Fig. 4. As explained in the text, although they exhibit one of two ‘archetypal’ forms that hardly change with depth in the corresponding stretches, their amplitude varies with depth (see colour scale) following the difference in δ between the vein and the mid-grain interior.

Movie S2. Evolution of horizontal isotopic pattern with depth in the simulation with $T = -32\text{ }^{\circ}\text{C}$, $\lambda = 10\text{ cm}$, $c = 5\text{ nm}$, $w = 0\text{ m yr}^{-1}$, and $D_b = 1.5 \times 10^{-11}\text{ m}^2\text{ s}^{-1}$ (high diffusivity run in Fig. 4a). The layout is the same as that in Movie S1.

Movie S3. Evolution of horizontal isotopic pattern with depth in the simulation with $T = -32\text{ }^{\circ}\text{C}$, $\lambda = 10\text{ cm}$, $c = 5\text{ nm}$, $w = 0\text{ m yr}^{-1}$, and $D_b = 1.5 \times 10^{-13}\text{ m}^2\text{ s}^{-1}$ (medium diffusivity run in Fig. 4c). The layout is the same as that in Movie S1.

Movie S4. Isotopic patterns from the run with $T = -32\text{ }^{\circ}\text{C}$, $\lambda = 10\text{ cm}$, $c = 5\text{ nm}$, $w = 5\text{ m yr}^{-1}$, $D_b = 1.5 \times 10^{-12}\text{ m}^2\text{ s}^{-1}$ (the run in Fig. 6b), compiled by sampling the solution at 50° tilt, with the tilt section meeting $z = z_2$ at $r = 0$ and the azimuth of the tilt axis varying from 0 to 360° . The patterns are shown here as they would appear when viewed along the tilt axis, instead of being reprojected onto the horizontal plane (as done in Fig. 11). The same protocol is used in Movies S5 to S7.

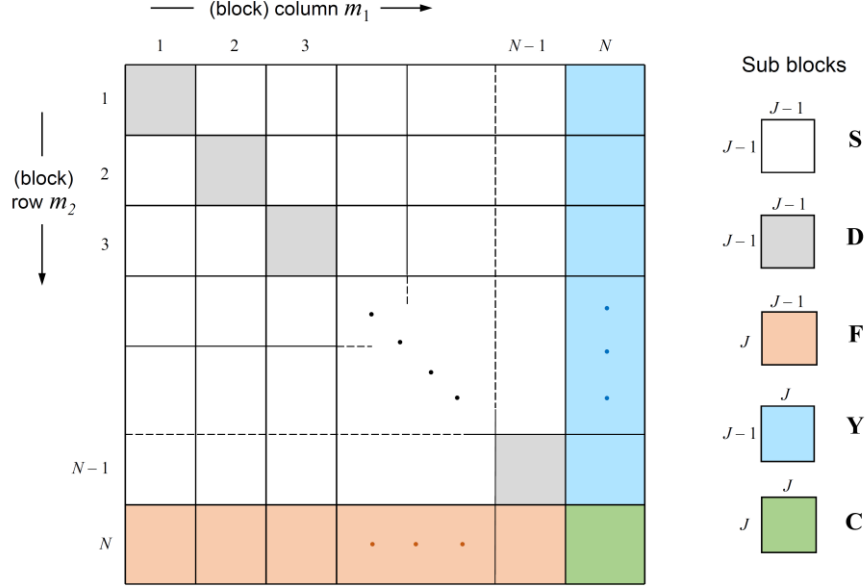
Movie S5. Isotopic patterns in the run with $T = -32\text{ }^{\circ}\text{C}$, $\lambda = 10\text{ cm}$, $c = 5\text{ nm}$, $w = 5\text{ m yr}^{-1}$, $D_b = 1.5 \times 10^{-11}\text{ m}^2\text{ s}^{-1}$ (Fig. 6a), from sampling the solution at 10° tilt, with the tilt section meeting $z = z_2$ at $r = 0$ and the tilt azimuth varying from 0 to 360° .

Movie S6. Isotopic patterns in the run with $T = -32\text{ }^{\circ}\text{C}$, $\lambda = 10\text{ cm}$, $c = 5\text{ nm}$, $w = 0\text{ m yr}^{-1}$, $D_b = 1.5 \times 10^{-11}\text{ m}^2\text{ s}^{-1}$ (Fig. 4a), from sampling the solution at 5° tilt, with the tilt section meeting $z = z_2$ at $r = 0$ and the tilt azimuth varying from 0 to 360° .

Movie S7. Isotopic patterns from the run with $T = -32\text{ }^{\circ}\text{C}$, $\lambda = 10\text{ cm}$, $c = 5\text{ nm}$, $w = 5\text{ m yr}^{-1}$, $D_b = 1.5 \times 10^{-11}\text{ m}^2\text{ s}^{-1}$ (Fig. 6a), from sampling the solution at 25° tilt, with the tilt section meeting $z = z_2$ at $r = 0$ and the tilt azimuth varying from 0 to 360° .

S1 Matrix \mathbf{M} in our numerical method

55 This section presents the elements of the matrix \mathbf{M} , which we derived from Eqs. (39) and (40) by using the mixed spectral and finite difference scheme of Sect 2.6. It is convenient to partition \mathbf{M} into $N \times N$ submatrices or blocks. There are five types of blocks, and we address each block's location in \mathbf{M} by the column and row indices m_1 and m_2 (Fig. S1).



60 **Figure S1.** Structure of block matrix \mathbf{M} . The key locates the five types of blocks defined in Eqs. (S3) to (S7) and indicates their sizes.

The radial step size from discretising the R -axis into J points (Fig. 3) is $\Delta = -\ln \zeta / (J - 1)$. Let us define the constants

$$\begin{aligned} c_1 &= -\frac{2\beta_b}{\Delta^2}, & c_2 &= \frac{\beta_b}{\Delta^2} - \frac{\beta_b + 1}{2\Delta}, & c_3 &= \frac{\beta_b}{\Delta^2} + \frac{\beta_b + 1}{2\Delta}, \\ c_4 &= \frac{2(\beta_b + 1)}{\Delta^2}, & c_5 &= (\beta_b + 1) \left(-\frac{1}{\Delta^2} + \frac{1}{2\Delta} \right), & c_6 &= (\beta_b + 1) \left(-\frac{1}{\Delta^2} - \frac{1}{2\Delta} \right) \end{aligned} \quad (\text{S1})$$

and the ingredient matrix

$$\mathbf{P} = \begin{bmatrix} e^{R_1 - 1} & & & \\ & e^{R_2 - 1} & & \\ & & \ddots & \\ & & & e^{R_{J-1} - 1} \end{bmatrix}. \quad (\text{S2})$$

Then, the blocks are given by

$$\mathbf{S}_{m_2, m_1} = -\frac{8(-1)^{N+m_1}}{\varepsilon \xi L(1+x_{m_1})} \mathbf{P}, \quad (\text{S3})$$

$$\mathbf{D}_{m_1 (=m_2)} = \mathbf{S}_{m_1, m_1} + \frac{1}{\Delta^2} \begin{bmatrix} 2e^{2(R_1-1)} & -2e^{2(R_1-1)} & & & \\ -e^{2(R_2-1)} & 2e^{2(R_2-1)} & -e^{2(R_2-1)} & & \\ & & \ddots & & \\ & & & \ddots & \\ & & & & -e^{2(R_{J-2}-1)} & 2e^{2(R_{J-2}-1)} & -e^{2(R_{J-2}-1)} \\ & & & & -e^{2(R_{J-1}-1)} & 2e^{2(R_{J-1}-1)} \end{bmatrix}, \quad (\text{S4})$$

$$\mathbf{F}_{m_1} (\text{rows } 1 \text{ to } J-1) = -\frac{8(-1)^{N+m_1}}{\varepsilon \xi L(1+x_{m_1})} \mathbf{P}, \quad \mathbf{F}_{m_1} (J\text{-th row}) = \begin{bmatrix} 0 & 0 & \cdots & -\frac{\pi p_2}{2\xi^2 N \Delta} \sqrt{1-x_{m_1}^2} \end{bmatrix}, \quad (\text{S5})$$

$$\mathbf{Y} = \begin{bmatrix} c_1 e^{2(R_1-1)} - \beta_b k_z^2 & -c_1 e^{2(R_1-1)} & & & \\ c_2 e^{2(R_2-1)} & c_1 e^{2(R_2-1)} - \beta_b k_z^2 & c_3 e^{2(R_2-1)} & & \\ & & \ddots & & \\ & & & c_2 e^{2(R_{J-2}-1)} & c_1 e^{2(R_{J-2}-1)} - \beta_b k_z^2 & c_3 e^{2(R_{J-2}-1)} \\ & & & c_2 e^{2(R_{J-1}-1)} & c_1 e^{2(R_{J-1}-1)} - \beta_b k_z^2 & c_3 e^{2(R_{J-1}-1)} \end{bmatrix}, \quad (\text{S6})$$

and

$$\mathbf{C}(\text{rows } 1 \text{ to } J-1) = \begin{bmatrix} c_4 e^{2(R_1-1)} + \beta_b k_z^2 & -c_4 e^{2(R_1-1)} & & & \\ c_5 e^{2(R_2-1)} & c_4 e^{2(R_2-1)} + \beta_b k_z^2 & c_6 e^{2(R_2-1)} & & \\ & & \ddots & & \\ & & & c_5 e^{2(R_{J-2}-1)} & c_4 e^{2(R_{J-2}-1)} + \beta_b k_z^2 & c_6 e^{2(R_{J-2}-1)} \\ & & & c_5 e^{2(R_{J-1}-1)} & c_4 e^{2(R_{J-1}-1)} + \beta_b k_z^2 & c_6 e^{2(R_{J-1}-1)} \end{bmatrix}$$

$$\mathbf{C}(J\text{-th row}) = \begin{bmatrix} 0 & 0 & \cdots & \frac{-1}{\xi^2 \Delta} (p_2 + \frac{p_3}{L}) & p_1 + \frac{1}{\xi^2 \Delta} (p_2 + \frac{p_3}{L}) \end{bmatrix}. \quad (\text{S7})$$

S2 Effect of reducing the signal wavelength to 2 cm

Figures S2 and S3 present the results of repeating the model runs in Figs. 4 and 6 with $\lambda = 2$ cm instead of 10 cm. The qualitative behaviour discussed in Sect. 3.1 for those runs – isotopic-pattern types and their influence by grain-boundary diffusivity and thickness – is essentially unchanged. However, the pattern amplitudes at $\lambda = 2$ cm are higher, reaching ≈ 0.1 – 0.3 times of the bulk-signal amplitude in those runs with lower values of D_b , as shown by the colour scales and isotopic profiles at far left.

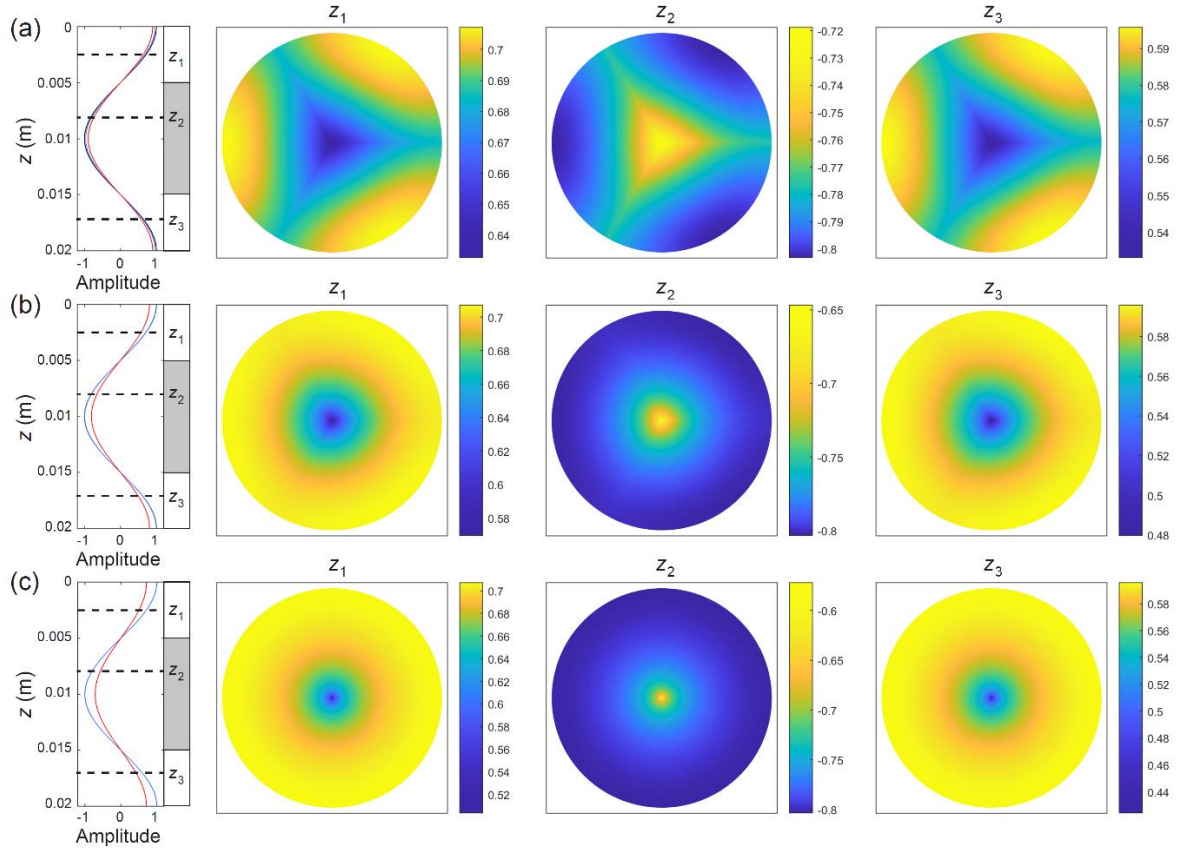


Figure S2. Isotopic patterns computed in three runs with $T = -32$ °C, $b = 1$ mm, $\lambda = 2$ cm, $c = 5$ nm, $w = 0$ m yr $^{-1}$, and $D_b =$ (a) 1.5×10^{-11} m 2 s $^{-1}$, (b) 1.5×10^{-12} m 2 s $^{-1}$, (c) 1.5×10^{-13} m 2 s $^{-1}$. This figure may be compared with Fig. 4, where $\lambda = 10$ cm; its layout follows the one in Fig. 4. In each far-left panel, curves show the depth profiles of the δ -variations at the mid-grain interior (black), grain-boundary interior (blue), and vein wall (red); the black curves in (b) and (c) are overlain by the blue. The enhancement factors in these runs are $f = 3.22, 2.42$, and 2.20 , respectively.

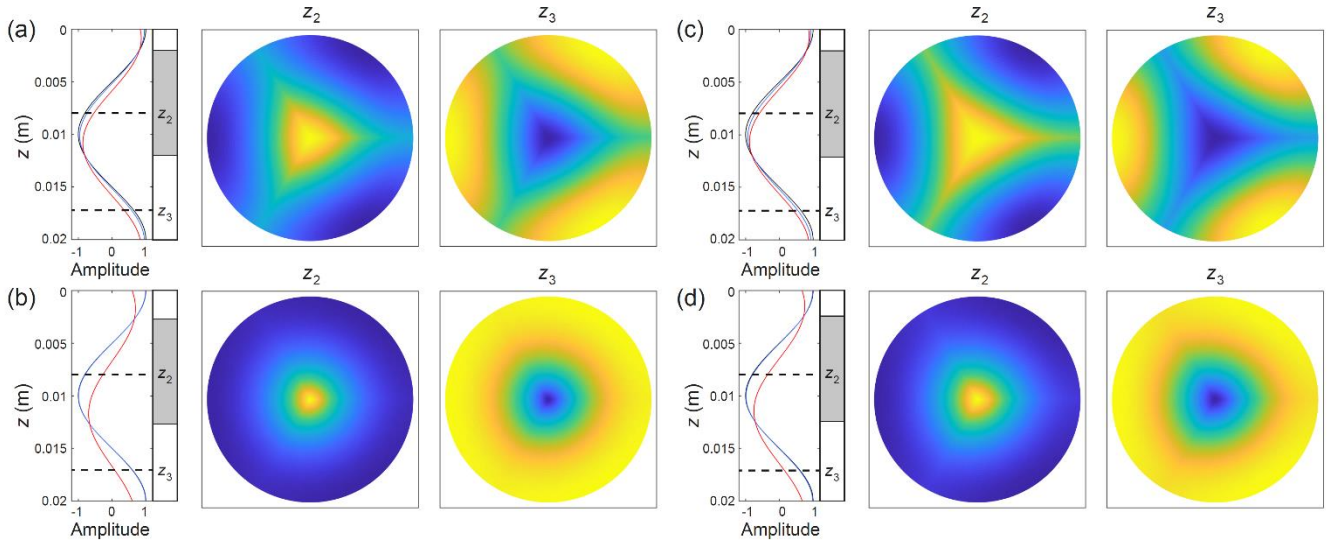


Figure S3. Archetypal isotopic patterns computed in four runs with $T = -32\text{ }^{\circ}\text{C}$, $b = 1\text{ mm}$, $\lambda = 2\text{ cm}$, $w = 5\text{ m yr}^{-1}$, and the grain-boundary properties: (a) $D_b = 1.5 \times 10^{-11}\text{ m}^2\text{ s}^{-1}$, $c = 5\text{ nm}$; (b) $D_b = 1.5 \times 10^{-12}\text{ m}^2\text{ s}^{-1}$, $c = 5\text{ nm}$; (c) $D_b = 1.5 \times 10^{-11}\text{ m}^2\text{ s}^{-1}$, $c = 10\text{ nm}$; (d) $D_b = 1.5 \times 10^{-12}\text{ m}^2\text{ s}^{-1}$, $c = 10\text{ nm}$. This figure may be compared with Fig. 6, where $\lambda = 10\text{ cm}$; its layout follows the one in Fig. 6. As in Fig. 6, the depths z_2 and z_3 are sampled, and we omit the colour range on each pattern, which is defined by the difference between the vertical isotopic profiles (curves at far left) for the mid-grain interior (black), grain-boundary interior (blue), and vein wall (red). The enhancement factors in these runs are $f =$ (a) 4.13, (b) 3.86, (c) 4.61, and (d) 3.92.

The following figures (Figs. S4 and S5) show that the archetypal pattern arrays reported in Sect. 3.1 for -32 and -52 °C (Figs. 9 and 10) are changed negligibly in the presence of vein-water flow. The enhancement factors f in Figs. S4 and S5 are included in Figs. 9 and 10 as red bracketed numbers.

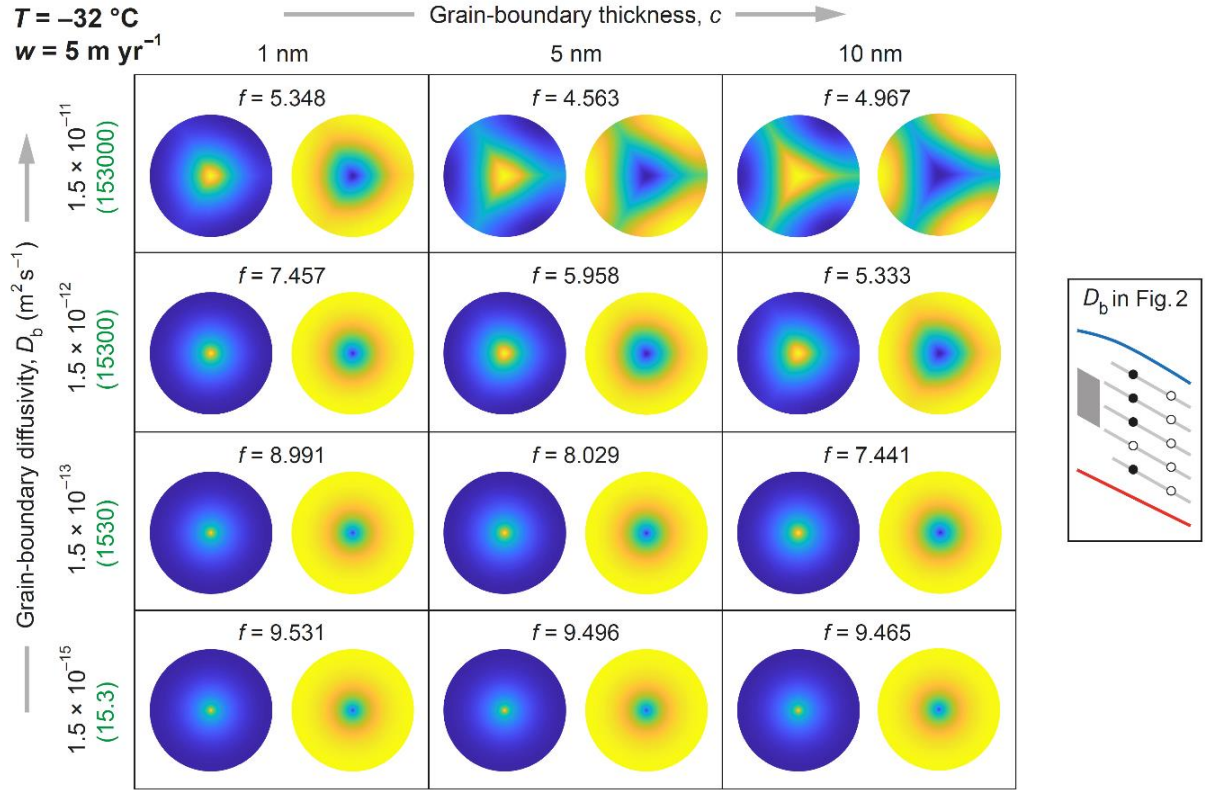


Figure S4. Dependence of archetypal patterns on grain-boundary diffusivity D_b and thickness c at -32 °C for $b = 1$ mm, $\lambda = 10$ cm, and $w = 5$ m yr $^{-1}$. Key on the right locates the four values of D_b as black filled circles on the scheme of Fig. 2. Numbers in green give the corresponding diffusivity contrasts β_b . Figure 9 presents analogous results for $w = 0$ m yr $^{-1}$.

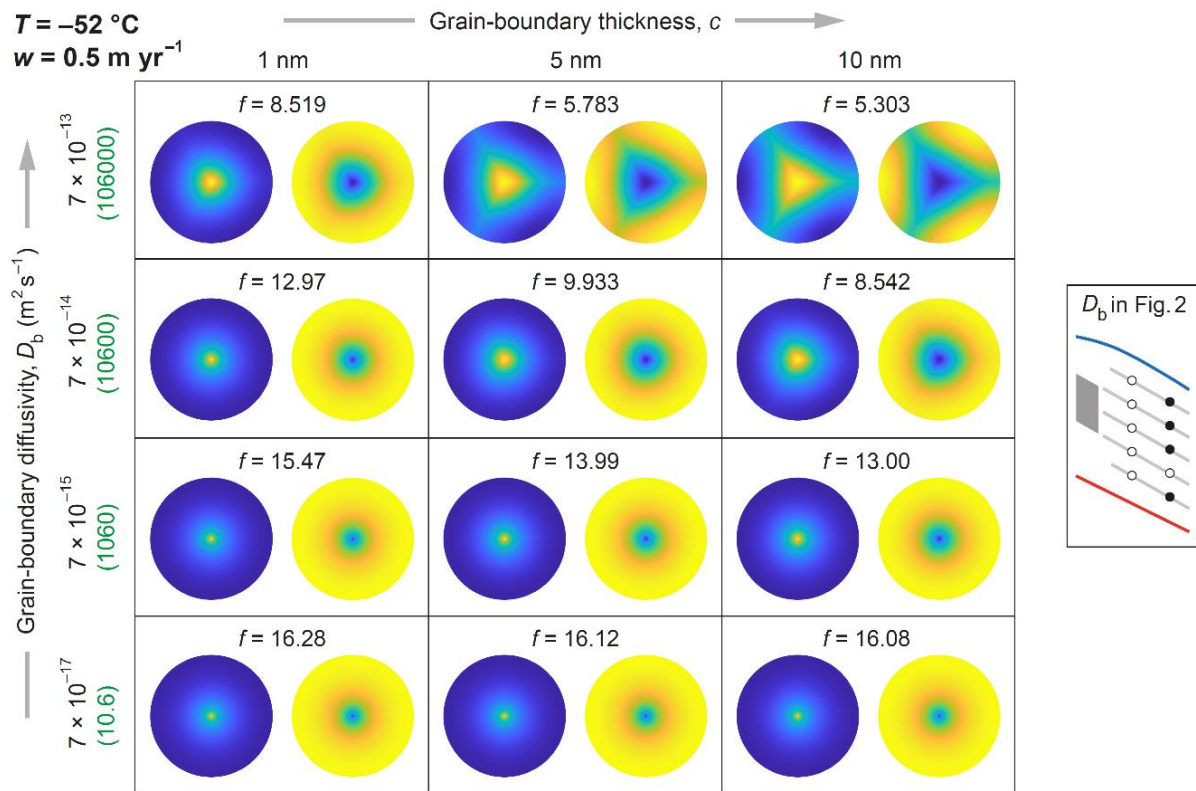


Figure S5. Dependence of archetypal patterns on grain-boundary diffusivity D_b and thickness c at $-52\text{ }^{\circ}\text{C}$ for $b = 1\text{ mm}$, $\lambda = 10\text{ cm}$ and $w = 0.5\text{ m yr}^{-1}$. Key on the right locates the four values of D_b as black filled circles on the scheme of Fig. 2. Numbers in green give the corresponding diffusivity contrasts β_b . Figure 10 presents analogous results for $w = 0\text{ m yr}^{-1}$.

S4 Effect of grain radius b larger than 1 mm

Figures S6–S9 present the results of repeating the runs in Figs. 4, 6, 9, and 10 with $b = 5$ mm instead of 1 mm. The range of behaviour discussed in Sect. 3.1 for those runs – the isotopic-pattern types, their influence by grain-boundary diffusivity and thickness, and the influence on the enhancement factor by vein-water flow – is broadly unchanged. Compared to those at $b = 1$ mm, the patterns at $b = 5$ mm are nearer the pole end of the pole-to-spoke continuum (i.e. with less-developed spokes) for the reason given in Sect. 3.1.3, but their isotopic excursions have widths amounting to a similar fraction (~ 10 –50 %) of the grain radius. Consequently, isotopic patterns on coarser-grain ice are wider and easier to resolve spatially. At $b = 5$ mm, the patterns also have greater amplitude, as shown by the isotopic profiles at far left in Figs. S6 and S7 (cf. Figs. 4 and 6).

Figure S10 shows the dependence of the enhancement factor f on grain radius b from 1 to 5 mm at -32 and -52 °C for different grain-boundary properties and vein-water flow conditions. The reason that f decreases (towards 1) with b is described in Sect. 3.2.

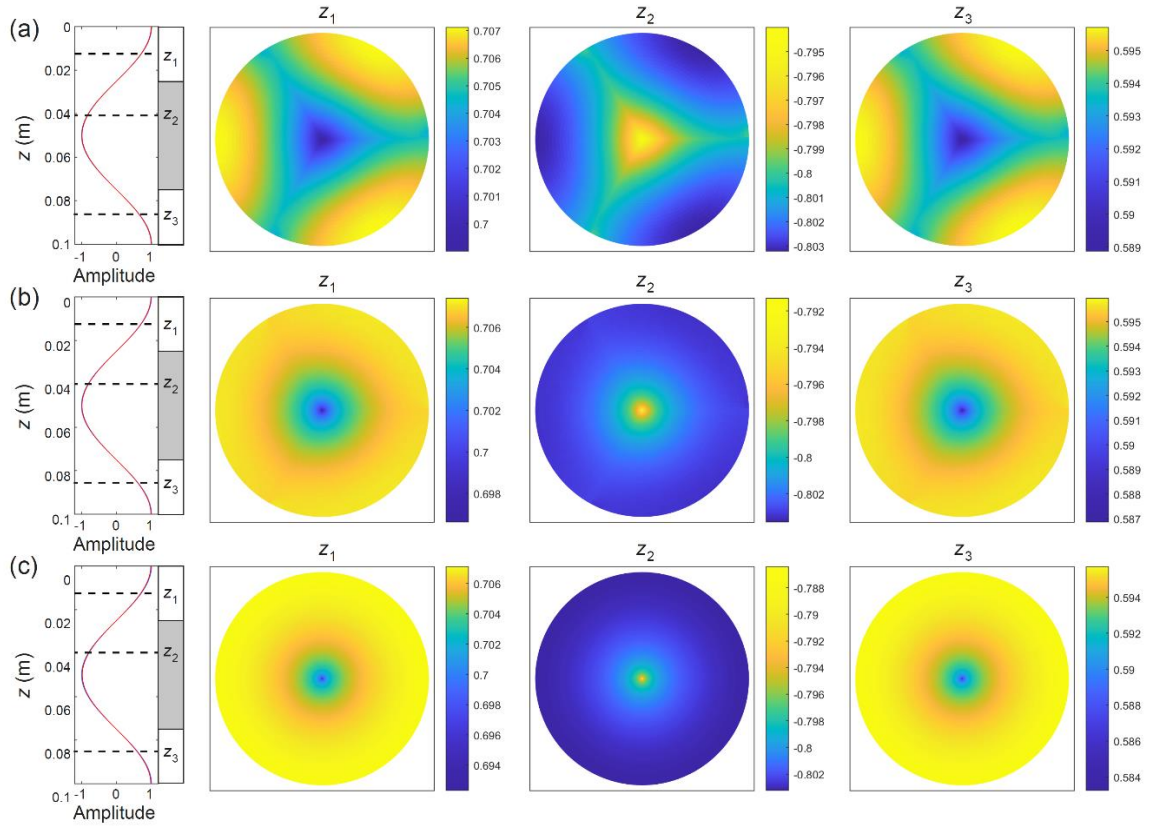


Figure S6. Isotopic patterns computed in three runs with $T = -32$ °C, $b = 5$ mm, $\lambda = 10$ cm, $c = 5$ nm, $w = 0$ m yr $^{-1}$, and $D_b =$ (a) 1.5×10^{-11} m 2 s $^{-1}$, (b) 1.5×10^{-12} m 2 s $^{-1}$, (c) 1.5×10^{-13} m 2 s $^{-1}$. This figure may be compared with Fig. 4, where $b = 1$ mm. The enhancement factors in these runs are $f = 1.217$, 1.074 , and 1.067 , respectively.

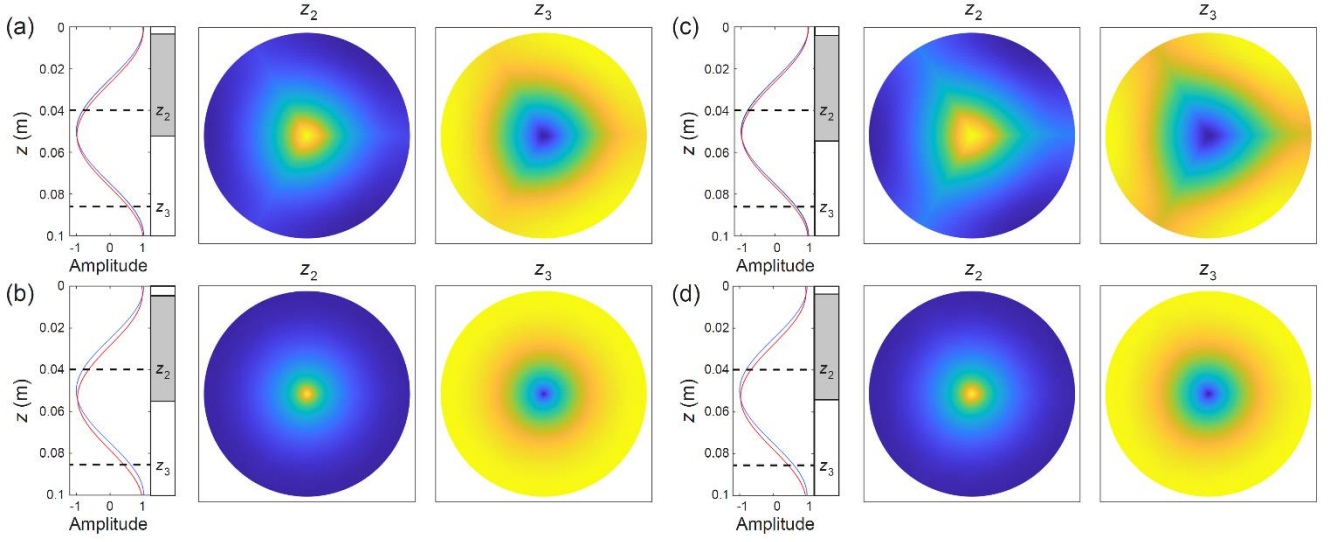


Figure S7. Archetypal isotopic patterns computed in four runs with $T = -32\text{ }^{\circ}\text{C}$, $b = 5\text{ mm}$, $\lambda = 10\text{ cm}$, $w = 5\text{ m yr}^{-1}$, and the grain-boundary properties: (a) $D_b = 1.5 \times 10^{-11}\text{ m}^2\text{ s}^{-1}$, $c = 5\text{ nm}$; (b) $D_b = 1.5 \times 10^{-12}\text{ m}^2\text{ s}^{-1}$, $c = 5\text{ nm}$; (c) $D_b = 1.5 \times 10^{-11}\text{ m}^2\text{ s}^{-1}$, $c = 10\text{ nm}$; (d) $D_b = 1.5 \times 10^{-12}\text{ m}^2\text{ s}^{-1}$, $c = 10\text{ nm}$. This figure may be compared with Fig. 6, where $b = 1\text{ mm}$. The enhancement factors in these runs are $f =$ (a) 1.293, (b) 1.263, (c) 1.412, and (d) 1.262.

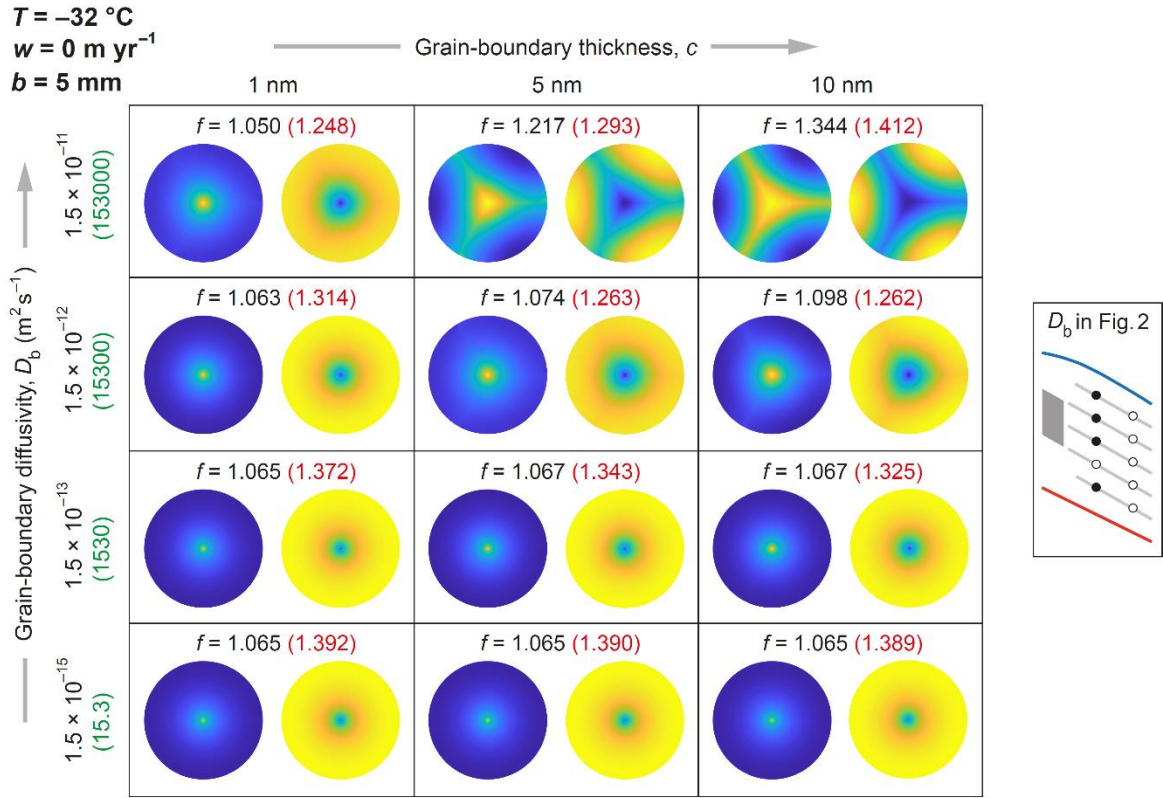
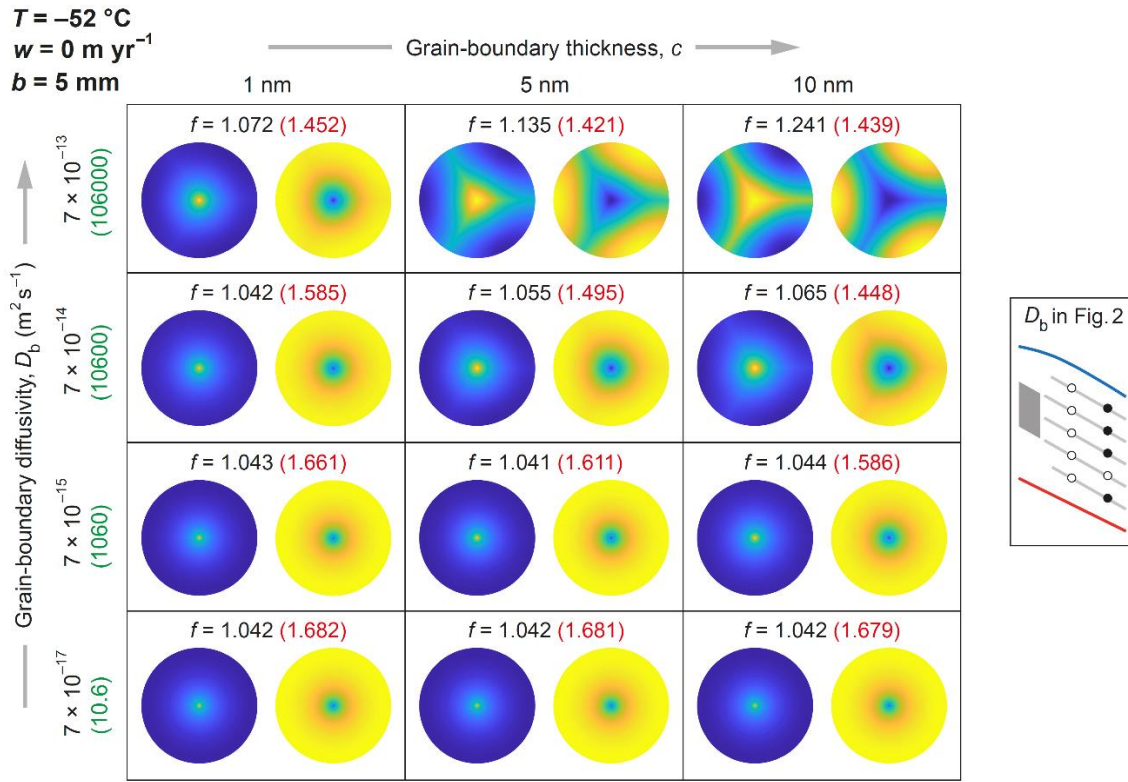


Figure S8. Dependence of archetypal patterns on grain-boundary diffusivity D_b and thickness c at $-32\text{ }^{\circ}\text{C}$ for $b = 5\text{ mm}$, $\lambda = 10\text{ cm}$, and $w = 0\text{ m yr}^{-1}$. The layout follows the one in Fig. 9, which presents analogous results for $b = 1\text{ mm}$. As in Fig. 9, the colour charts reach out to the grain radius (5 mm here); the isotopic patterns and the enhancement factors f in black are for $w = 0\text{ m yr}^{-1}$; and bracketed in red are the f -values when vein water flows at $w = 5\text{ m yr}^{-1}$, which produces patterns similar to the ones shown.



165 **Figure S9.** Dependence of archetypal patterns on grain-boundary diffusivity D_b and thickness c at $-52\text{ }^{\circ}\text{C}$ for $b = 5\text{ mm}$, $\lambda = 10\text{ cm}$ and $w = 0\text{ m yr}^{-1}$. The layout follows the one in Fig. 10, which presents analogous results for $b = 1\text{ mm}$. As in Fig. 10, the colour charts reach out to the grain radius (5 mm here); the isotopic patterns and the enhancement factors f in black are for $w = 0\text{ m yr}^{-1}$; and bracketed in red are the f -values when vein water flows at $w = 0.5\text{ m yr}^{-1}$, which produces patterns similar to the ones shown.

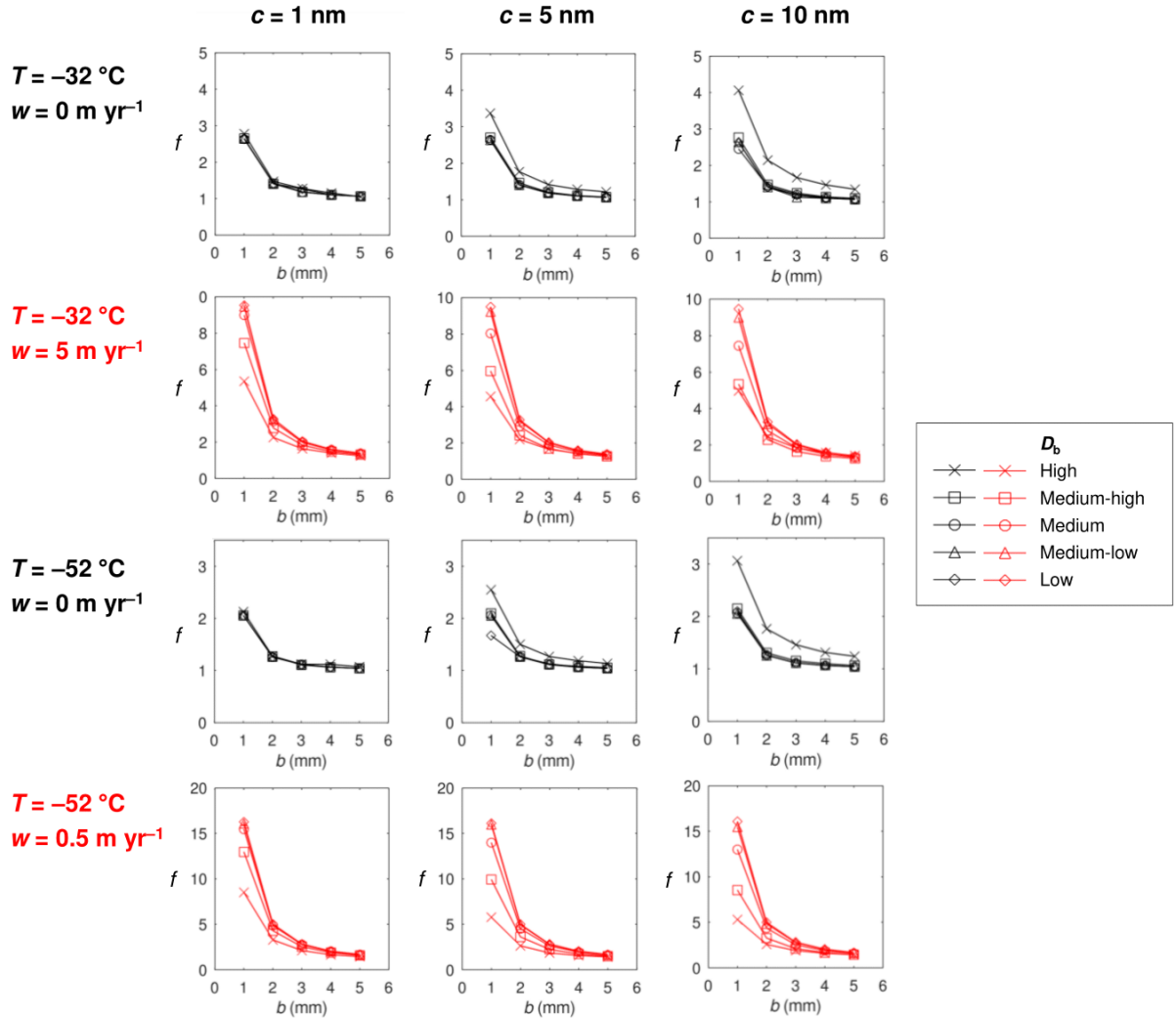
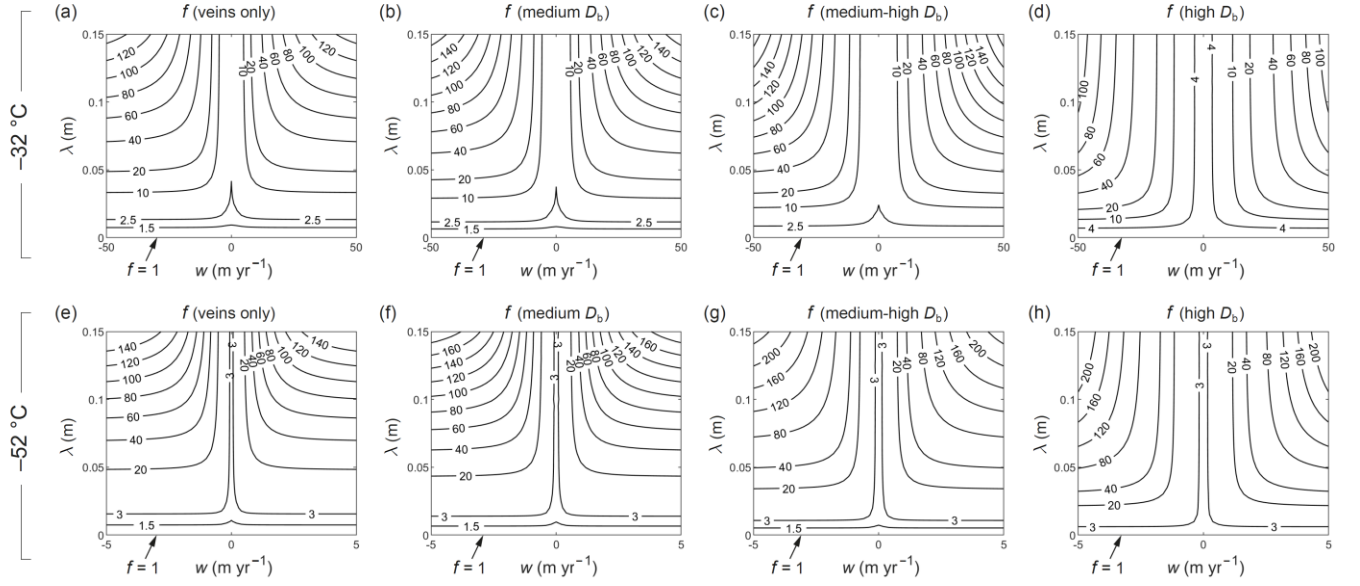


Figure S10. Enhancement factor f on the bulk-ice diffusivity as a function of grain radius b from 1 to 5 mm in 1-mm increments, for the signal wavelength $\lambda = 10$ cm and for different grain-boundary thicknesses c (1, 5, 10 nm: left, middle and right-hand columns of panels, respectively), temperatures T , and vein-water flow velocities w (see label on the left on each row of panels). Results for $w = 0$ are plotted in black; for $w > 0$, in red. The key lists the plot symbols for different values of the grain-boundary diffusivity D_b on our descriptive scale.



180 **Figure S11.** Impact of the presence and diffusivity (D_b) of grain boundaries on the level of excess diffusion for different vein-flow velocities w and signal wavelengths λ at -32°C and -52°C when $b = 1\text{ mm}$ and $c = 5\text{ nm}$. (a, e) Contour maps of the enhancement factor $f(w, \lambda)$ for the vein-only system without grain boundaries; data from Ng (2023). (b–d) Contour maps of f at -32°C when D_b is medium, medium-high, and high. (f–h) Contour maps of f at -52°C when D_b is medium, medium-high, and high.